Title
TARGET RESIDUES FROM THE REACTION OF 8 GeV 20Ne WITH 181Ta AND 197Au

Author
Morrissey, D.J.

Publication Date
1979-05-01

LBL-8983
Preprint

Lawrence Berkeley Laboratory
UNIVERSITY OF CALIFORNIA, BERKELEY, CA

Submitted to Physical Review C

TARGET RESIDUES FROM THE REACTION OF 8 GeV ^{20}Ne WITH ^{181}Ta AND ^{197}Au

D. J. Morrissey, W. Loveland, M. de Saint Simon,
and G. T. Seaborg

May 1979

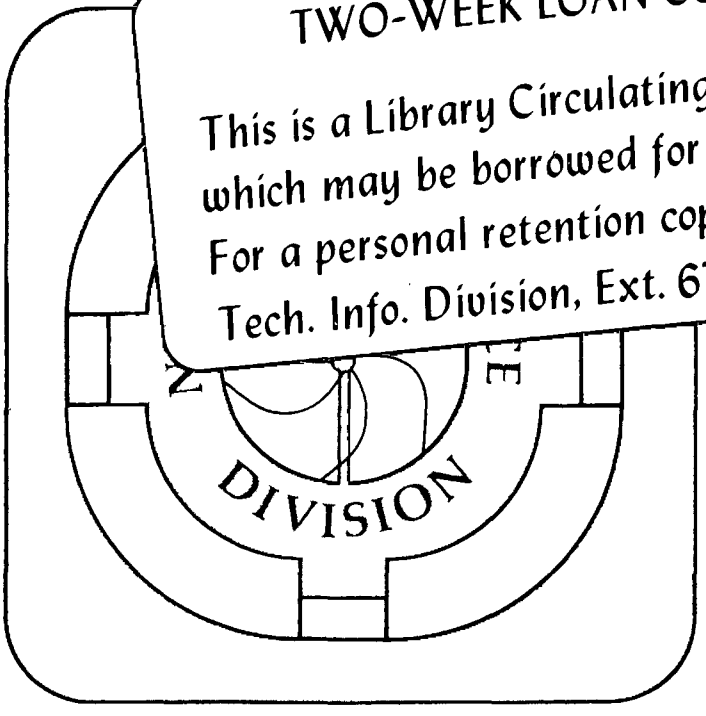

Prepared for the U. S. Department of Energy
under Contract W-7405-ENG-48

DISCLAIMER

LBL-8983

TARGET RESIDUES FROM THE REACTION OF 8 GeV ^{20}Ne WITH ^{181}Ta AND ^{197}Au*

D. J. Morrissey, W. Loveland**, M. de Saint Simon***, and G. T. Seaborg

Lawrence Berkeley Laboratory, University of California
Berkeley, CA 94720

ABSTRACT

The cross sections for the production of 109 different target fragments from reactions of 8.0 GeV ^{20}Ne with ^{181}Ta and ^{197}Au were measured. The target fragment radioactivities were measured by off-line gamma ray spectroscopy. Details of the measurement as well as the calculation of the independent isotopic production cross sections ($d^2\sigma/dZdA$) and the integrated mass yields ($d\sigma/dA$) are given. Comparisons of these data to previously reported data for proton induced reactions show that the target residue production cross sections scale with the total projectile energy, not velocity. The total cross section for residue production indicates that some products result from collisions with significant overlap of the central densities of the two nuclei, in contrast to results obtained with low mass targets. Comparisons of the data with a Monte Carlo cascade calculation and an abrasion-ablation calculation verify the importance of ground state correlations of the neutrons and protons on the fragmentation isotopic cross sections.

NUCLEAR REACTIONS: ^{181}Ta (^{20}Ne, spallation), ^{197}Au(^{20}Ne, spallation), E = 8.0 GeV; measured radionuclide production cross sections ($d^2\sigma/dZdA$) and $d\sigma/dA$; comparison to proton induced spallation of ^{181}Ta and ^{197}Au; comparison to abrasion-ablation and Monte Carlo cascade models for residue production; Ge(Li) spectroscopy, radioanalytical mass and charge distributions; relativistic heavy ion nuclear reactions.

I. INTRODUCTION

Currently the highest kinetic energy available for the laboratory study of heavy ion induced reactions is 2.1A GeV.[1] Reactions induced by these heavy ions were thought to hold great promise for the observation of many exotic collective phenomena not observable in proton induced reactions.[2] A large body of data now exists from the study of 25 GeV ^{12}C ions interacting with targets ranging from hydrogen to uranium.[3-8] Both radiochemical and on-line counter techniques have been successfully employed in these studies. The experimental observables have been found to separate into three major categories according to the rapidity of the products: projectile fragments tightly correlated with the beam rapidity,[3] from large impact parameter peripheral collisions; light products, such as protons, alphas and pi mesons, moving with intermediate rapidities and showing evidence of thermalization,[4] from central collisions; and large target residues that do not escape the target materials and thus have low rapidities,[5-8] from peripheral and near central collisions. These studies have shown no evidence for the predicted exotic phenomena that spurred them on, and now the suggestion is that still higher energies are necessary for the observation of such phenomena.[9] Such energies are not presently available; however, many facets of the reaction mechanisms at the currently available heavy ion energies are not well known. And so, attention is now being turned toward understanding the relationship of heavy ion reactions at a few GeV per nucleon to the well explored fields of low energy heavy ion reactions and relativistic proton induced reactions.

The previous studies of relativistic heavy ion (RHI) induced reactions have shown the production, in large amounts, of "heavy" target residues.[5-8,10] These residues range in mass from essentially that of the target down to the lightest nucleus observable with the radiochemical methods employed, ^{7}Be. The residue production cross section has been found to be ∿70 percent of the geometrical reaction cross section for both low and high mass targets. Observation of such products is not expected for central collisions of the projectile and target and thus such results set a limit on the number of true central collisions. An important aspect of these studies will be to determine if the number of central collisions, i.e. collisions resulting in the complete annihilation of the target nucleus, is dependent on the projectile velocity. Due to the extreme velocity of the RHI projectiles the total reaction cross section does not vary significantly over this energy region. Up to the present only one study of target residue production in RHI reactions at an energy lower than 2.1 GeV/nucleon has been reported,[11] that for the reaction of 280 MeV/nucleon ^{14}N with copper. However, only relative yields for target residue products were reported for this system. Thus, the assumption of straight line trajectories that forms the basis of the fireball[4] and firestreak[12] models remains untested over a wide energy region of its assumed applicability.[4,13]

A second question of basic interest in RHI induced reactions is how such reactions compare with relativistic proton induced reactions. It has become common when discussing the projectile-like and intermediate products from RHI induced reactions to describe the experiments in terms of the projectile velocity (i.e. 2.1 GeV/nucleon, etc.).[3,4,13]

Relative yield measurements by Cumming et al.[5,11] have shown that the target residue isotope production cross sections, $d^2\sigma/dZdA$, for the interaction of 3.9 GeV ^{14}N and 25.2 GeV ^{12}C with copper targets compare most favorably with isotope production cross sections from reactions induced by protons of equivalent total energy. However, another study by Cumming et al.[10] showed that the target residue isotope production cross sections from the reaction of 80 GeV ^{40}Ar with copper also compared very favorably with those from the reaction of 28 GeV protons with copper. In view of the observed difference between 25 GeV ^{12}C induced reactions on high mass[8], ^{238}U, and low mass[5], Cu, targets and the larger volume to surface ratio in high mass targets, we felt it was important to study the relative importance of velocity and total energy in RHI interactions with heavy nuclei. A particularly good target nucleus for this comparison is ^{181}Ta. Previous studies of the reaction of 340 MeV protons with ^{181}Ta by Nervik and Seaborg,[14] and the reaction of 5.7 GeV protons with ^{181}Ta by Grover[15] showed large differences between the product mass distributions, $d\sigma/dA$, for these two reactions (see in Fig. 1). The comparison between the mass distribution from the reaction of 8 GeV ^{20}Ne with ^{181}Ta with these distributions should allow differentiation between the velocity and total energy dependence of RHI induced reactions with a ^{181}Ta target.

In this paper we report the study of the reaction of 400 MeV/A ^{20}Ne projectiles (8.0 GeV total energy) with ^{181}Ta and ^{197}Au targets. As discussed above the choice of this projectile and energy allows us to make the comparison with the earlier studies of the proton induced

reactions and also allows us to study the interaction of RHI at an energy lower than the previously reported studies. In section II we present the details of the experimental procedure used in this work and in section III we present the results. The results are compared to abrasion-ablation model calculations[16-18] from which we are able to draw conclusions on the ability to observe the predicted ground state correlations of nuclear matter.[18,19] Part of this work was published previously in a preliminary form.[20]

II. EXPERIMENTAL

A. Cross Section Measurement

As in previously reported radioanalytical measurements of the target residue products from RHI reactions,[6-8,14] these products are observed through gamma-ray spectroscopy of the target materials subsequent to the irradiation. A detailed review of the reproducibility and sources of error in such measurements has been made by Orth et al.[21] and the considerations of Cumming[22] for proton induced reactions certainly apply here. The ^{197}Au targets consisted of two foils, 12.5 cm by 10.2 cm each, with thicknesses 49.3 mg/cm^2 and 242.0 mg/cm^2, each surrounded by 6.6 mg/cm^2 Al catcher foils. These two targets, differing by a factor of approximately 5 in thickness, allowed us to evaluate the contribution from secondary particle induced reactions to the RHI reaction products. The ^{181}Ta target consisted of a single foil, 13.6 cm by 10.2 cm, of thickness 154.1 mg/cm^2, also surrounded by 6.6 mg/cm^2 Al foils. An external beam of ^{20}Ne was delivered to a $\sim$1 m air gap by the Bevalac at the Lawrence Berkeley Laboratory. Two separate irradiations were performed, one of the gold foils and one of the tantalum foil. The average beam fluxes and durations of these irradiations are given in Table I. The beam intensity was monitored on a pulse by pulse basis with a Ar-CO_2 ion chamber (80% Ar, 20% CO_2) that was developed and calibrated for use at the Bevalac facility.[23] In order to check the reproducibility of the ion chamber calibration and to facilitate absolute normalization of the calibration, aluminum monitor foils were irradiated in series with the primary target foils and the ionization chamber.

These aluminum monitor foils were 20.3 mg/cm^2 thick and were surrounded by 5.6 mg/cm^2 Mylar catcher foils. A schematic diagram of the arrangement of the target foils, monitor foils and ion chamber in the air gap irradiation facility is shown in Fig. 2. The beam enters from the left and passes through the ion chamber, the primary target materials, and then through the Al monitor foil. Approximately 30 m ahead of the targets the beam is bent $\sim 5^{o}$ clockwise and approximately 2 m ahead of the targets it is bent $\sim 10^{o}$ further clockwise to remove contaminants from the beam.

Approximate values for the energy loss of the 8.0 GeV ^{20}Ne beam in each of the primary targets are given in Table I. The $^{20}Ne^{10+}$ ions are near minimum ionizing at this energy[24] and approximate values of the energy loss can be obtained from the Bethe formula.[25,24] As one can see from Table I the energy lost by the ^{20}Ne beam in all the targets is quite small and for the purposes of this work can be ignored. Estimates of the attenuation of the beam by nuclear reactions are also given in Table I. These values of ϕ'/ϕ, the emergent flux divided by the incident flux, were calculated from the total reaction cross sections of Heckman et al.[26] Again, these estimates show that the beam is only slightly degraded by passage through the target materials, and therefore nuclear attenuation of the beam also can be ignored.

Gamma-ray spectrometric measurements were made with a single Ge(Li) detector on $\sim$5-10 cm^2 area pieces cut from the irradiated target foils, which were centered on the beam spot. These measurements began $\sim$20 minutes after the end of bombardment (EOB) for the gold targets, $\sim$14 hours after EOB for the tantalum target, and continued essentially

uninterrupted for ∿40 days. The identification of the product radioactivities and the calculation of their production cross sections has been described in detail elsewhere,[27] and will only be described briefly here. After the gamma-ray measurements were completed the spectra were analyzed with an automatic version of SAMPO.[28,27] This code performs a peak-find, a peak-fit and then an energy calculation and a full energy peak efficiency correction for each spectrum. Decay curves are then automatically constructed with the sorting routine TAU1. These decay curves are then identified interactively by their gamma-ray energy and half-life with the code TAU2. Multiple assignments are made to the decay curves at this point if the assignment based on the combination of half-life and gamma-ray energy is ambiguous. Off-line, all the assignments are screened to remove multiple assignments and insure that the gamma-rays for each isotope were observed with the proper abundances (i.e. no transition stronger than the observed transition can be missing). The cross section is then calculated from the statistically weighted average of the observed gamma-ray transitions for each isotope.

The cross section calculation includes corrections for a non-uniform beam level during the irradiation. During the bombardment of the ^{197}Au targets 2.4 percent of the beam was delivered in the first 175 minutes, and the second 97.6 percent was delivered in the final 416 minutes, with a 21 minute interruption in between. A constant beam level was maintained during the bombardment of the ^{181}Ta target. The production cross sections for all the activities observed in this work are given in Table II. The cross sections and their uncertainties due to counting statistics are given in millibarns for each nuclide

observed in each of the three targets. The nuclide type, I or C, indicates whether the cross section is an independent yield or a partial cumulative yield, respectively. Seventy-seven different radioactivities were observed in the two gold targets (36 in the thinner target and 66 in the thicker target which includes those observed in both) and 74 radioactivities were identified as reaction products in the tantalum target. In all, 109 different radioactivities were identified.

The contribution of secondary particle induced reactions to the measured cross sections can be estimated from a comparison of the production cross sections measured with the 49.3 mg/cm^2 ^{197}Au target to those measured with the 242.0 mg/cm^2 ^{197}Au target. Cumming et al. have previously reported a study of the secondary reaction contributions to the products from the reaction of the 28 GeV protons and 25 GeV ^{12}C ions with copper.[5] In their study they found that the secondary contributions to cross sections measured using two targets of total thickness 154 mg/cm^2 and 1158 mg/cm^2 differed by factors that ranged from no contribution to 23 percent with the proton projectiles (the highest contributions were to near-target products). Estimates of the increase in secondary contributions with the ^{12}C projectiles over the protons ranges from a factor of $\sim$1 to $\sim$3 when measured with only the thicker copper target.[5] Novel arguments were used also by Cumming et al. to conclude that secondary contributions for 80 GeV ^{40}Ar projectiles, for all but the lightest products, were proportional to those found from proton reactions.[11] The thin target used in the present study was nearly a factor of 3 thinner than the thinnest targets used in obtaining the previously reported estimates of Cumming et al.[5,11]

and secondary contributions in this foil should be negligible.

A simple way to obtain a feeling for the variation and importance of secondary reaction contributions to the cross sections measured with the thicker ^{197}Au foil is to plot the ratio of measurements versus product mass number. This has been done in Fig. 3 (uncertainties represent one standard deviation), and the values of the ratios are given in Table III for the 24 products observed in both foils. Figure 3 shows that no dramatic variation of the ratio of the measured cross sections can be seen as a function of product mass number. A least squares analysis shows that the linear function $R = 1.044 - 6.0 \times 10^{-4} A$ gives a slightly better description of the data than a straight line at R = 1. This function is shown by the dashed line in Fig. 3. The statistical F test of the inclusion of the mass number dependence of the ratio yields a value of $F_\chi = 9.2$, which also indicates that such a dependence may be justified by the data.[29] However, because all the data points (save two) are within one standard deviation of R = 1, contributions from secondary reactions to the production cross sections were ignored.

B. Charge and Mass Distributions

The radiochemical cross sections, whose measurement was described above, represent post neutron and charged particle evaporation, post "fast" beta decay production cross sections. Thus, in order to obtain true production cross sections one needs to correct radiochemically measured cross sections for beta decay, when possible, that occurs between the time of their production in the nuclear reaction and the time at which they are detected through their own beta decay. Once

corrected these values of the independent production cross sections, $d^2\sigma/dZdA$, can be used to calculate the mass or charge yield, $d\sigma/dA$ or $d\sigma/dZ$ respectively, and also to estimate the total cross section for target residue production.

In order to make the correction for precursor decay to each measured cross section and in order to calculate the total isobaric or mass yield we have used the assumption of Gaussian charge dispersions. That is, the independent yield cross sections can be represented by a histogram that lies along a Gaussian curve, at constant mass number. This is written:

$$\frac{d^2\sigma}{dZdA} = \frac{d\sigma}{dA}\left\{(2\Pi s_z(A)^2)^{-1/2} \exp\left[\frac{(Z - Z_p(A))^2}{-2s_z(A)^2}\right]\right\} \quad (1)$$

with the three parameters: $d\sigma/dA$, the total isobaric yield, $s_z(A)$, the Gaussian width parameter, and $Z_p(A)$ the most probable Z value for that isobar. Given the assumption of Gaussian charge dispersions, the beta decay feeding correction factors for cumulative yield isobaric members can be calculated once the centroid and width of the Gaussian are known.

In order to uniquely specify these three variables $\frac{d\sigma}{dA}$, $s_z(A)$ and $z_p(A)$ one would need to measure more than three independent yield cross sections for each isobar. But, there are no isobaric chains that contain three members that are shielded from beta decay. In fact, the nature of radioanalytical studies such as this one does not, in general, lend itself to the measurement of isobaric members. Rather, a wide assortment of radioactivities are observed which span the entire range of the periodic table that is accessible in the nuclear

reaction. As a result relatively few isobaric pairs are observed.[5-8,10,11] A further assumption needs to be introduced in order to apply the Gaussian charge distributions to the measured data. The assumption is, that the value of $d\sigma/dA$ varies smoothly and slowly as a function of mass number, A. This assumption is not as severe as the assumption that the production cross sections for RHI reactions follow the Rudstam systematics[30] for proton induced reactions that has been used in the analysis of data from low mass targets by Cumming et al.[5,10,11] Another statement of the former, less stringent, assumption is that the charge dispersion curves for neighboring isobaric chains should be similar, thus, radionuclide yields from a limited mass range can be used to determine a single charge dispersion curve. The two Gaussian parameters that specify the width, $s_z(A)$, and the center $Z_p(A)$, of the charge distributions are iteratively fit to the measured data over limited mass regions. The width parameter has been found, in general, to be approximately independent of mass number over small ranges of A. The center of the charge dispersions were adequately represented by linear functions in A, over small ranges of A, with the exception that an A^2 term was needed for the highest mass regions. The width parameters and the coefficients of the $Z_p(A)$ function are given in Table IV. These parameters should not be considered as absolutes but rather as a consistent set.

The results of this procedure can be seen in Figs. 4 and 5, where the calculated isotopic production cross sections are plotted versus $Z - Z_p(A)$, the distance in Z units from the center of the isobaric charge dispersion. Also shown in Figs. 4 and 5 are the Gaussian curves

that are specified by equation (1) with the parameters in Table IV, appropriately calculated for histogram distributions in Z. The data from the reaction of ^{20}Ne with ^{181}Ta and ^{197}Au are found to lie along the same charge dispersion curves for low mass products, but as one gets closer to the mass of the targets the two distributions separate. An interesting feature of this comparison is that, as shown in Fig. 4, the low mass products from this reaction have the same charge dispersion width as the same products from RHI reactions with copper targets[10,11,31] but in this work are shifted towards the neutron excessive side of the valley of beta stability. Such comparisons will be discussed in the next section.

The value of the isobaric or mass yield is obtained for each data point through the assumption of Gaussian charge dispersions and the set of parameters in Table IV. The measured production cross sections are adjusted to remove precursor feeding, where necessary, and a set of independent yield production cross sections, seen in Figs. 4 and 5, is generated. The mass yield is then calculated as the independent yield cross section divided by the fractional chain yield. The mass yields obtained in this manner are shown as the solid points in Figs. 6 and 7.

III. RESULTS AND DISCUSSION

It is convenient to divide the presentation of the results into two parts. In the first part the mass distribution results are presented and discussed in terms of their implications for limiting fragmentation, and their relation to the total reaction cross section. In the second part comparisons of the predictions of different models of RHI reactions are compared to the detailed isotopic production cross sections for near target residues. These comparisons will shed light on the question of correlations of neutrons and protons in the nuclear ground state.

A. Mass Yield Results

Comparison of the mass distribution from the reaction of 8.0 GeV ^{20}Ne with ^{181}Ta with the previous studies of proton induced reactions,[14,15] seen in Fig. 6, shows the striking agreement of the RHI results with those from proton induced reactions of the (approximately) equivalent total projectile energy. This agreement is confirmed by the comparison of the ^{20}Ne + ^{197}Au mass distribution with the results of Kaufman et al.[32] for the reaction of 11.5 GeV protons with ^{197}Au and the sparser results of Hudis et al.[33] for gaseous products from the reaction of 29 GeV protons with ^{197}Au. This comparison can be seen in Fig. 7. Although no complete study of the reaction of $\sim$400 MeV protons with ^{197}Au exists, the mass distribution is expected to be similar to that obtained with ^{181}Ta targets.[34]

The agreement of the ^{20}Ne + ^{181}Ta and ^{197}Au mass distributions with those produced by high energy protons can be viewed as a manifestation of limiting fragmentation, as the studies with copper targets have been viewed.[10] This process whose origins stem from high energy

physics,[35] has been extensively invoked and verified in studies of projectile fragments in RHI reactions.[26,36] The fact that the general features of the mass distributions from the reaction of 8.0 GeV ^{20}Ne and 29 GeV protons with ^{197}Au are so similar, even though differing widely in projectile energy, would also lend support to the limiting fragmentation hypothesis. However, similarity of these final distribution of products does not necessitate similarity of the primary excited systems, as suggested in reference 10 from the study of copper fragmentation. On the contrary, Morrissey et al.[37] have shown that strongly divergent distributions of primary products and excitation energies can, in fact, lead to essentially the same final product distributions for light fragmenting nuclei. This can be attributed to the dominance of the statistical phase of the deexcitation process on the distribution of the final product cross sections in the same way as the momentum distributions of projectile fragments were shown to be dominated by the Fermi momentum.[38] However, these results should be recognized as indicating that little, if any, change can be expected in the mass distribution if the projectile energy is increased.

Integration of the mass yield curves, $d\sigma/dA$, over mass number gives the cross section for the production of target residues. We have chosen to integrate these curves over the interval from mass number 40 to the mass of the target. We have chosen a lower limit of 40 mass units for several reasons, (a) the multiplicity of fragments with masses smaller than $\sim$40 is unknown, that is, these products may arise from interactions where another heavy fragment also survives. This certainly is true for fragments such as protons and ^{4}He, where

the number of such fragments per event is much greater than one.[4] And (b), because in studies such as this one very little data exists for these low mass products.

The results of this integration are contained in Table V. The total cross sections for the production of heavy target residues from ^{181}Ta and ^{197}Au were found to be 2.8 $\pm$ 0.5 barns. The fact that a small difference that would be expected on the basis of mass number difference was not seen between the two targets is due to the scatter in the calculated mass yields. For comparison we have included two calculations of the total reaction cross section in Table V. The hard sphere calculation refers to the overlap form of the sharp sphere model where the total reaction cross section is written:[39]

$$\sigma_R = \pi r_o^2 \, (A_T^{1/3} + A_p^{1/3} - b_{Tp})^2. \qquad (2)$$

We have taken the parameters r_o and b_{Tp} to be 1.37 fm and 0.51 fm, respectively, from the work of Heckman et al. on projectile fragmentation.[26] The soft sphere calculations are those of Karol which were developed to take into account both the diffuse nuclear surface and the variation of the nucleon-nucleon cross section with energy.[40] The comparison of the hard sphere calculations with our measured heavy fragment cross sections show that approximately 75 percent of the reaction cross section gives rise to these products. The soft sphere calculation would indicate that these products represent approximately 80 percent of the reaction cross section.

A current working hypothesis is that target residues are produced in peripheral reactions.[17-19] An estimate of the impact parameter range that gives rise to these products can be made from the fraction of the total reaction cross section that they represent. Thus, 75 percent of the hard sphere reaction cross section would lie between the impact parameter range of $0.5\ (R_T + R_p) \leqslant b \leqslant (R_T + R_p)$. This indicates that heavy residues are created in collisions where the center of the projectile lies inside the radius of the target nucleus. This situation is significantly different from the reaction of ^{40}Ar with ^{Nat}Cu where no target residues were inferred to arise from such central collisions.[10]

B. Comparisons with Reaction Model Calculations

Presently there are two models of the collision process that occur in RHI reactions that have been used to calculate isotopic and mass yield cross sections. They are a microscopic intranuclear cascade model of Yariv and Fraenkel[41] and the macroscopic abrasion-ablation model.[16-19] The predictions of these reaction models for the fragmentation of 213 MeV per nucleon ^{40}Ar has shown that the statistical deexcitation of the highly excited primary reaction products plays the dominant role in determining the product mass distributions in both calculations.[37,42] A comparison of these two calculations has also been made for the target residues produced in the reaction of 25 GeV ^{12}C with ^{Nat}Ag.[43,42] In this latter comparison, as with the comparison for ^{40}Ar, the mass yield curve was well reproduced by both calculations. However, unlike the ^{40}Ar fragmentation calculations, the isotopic production cross sections, $d^2\sigma/dZdA$, from the two calculations

were not at all similar. The Monte Carlo cascade calculation consistently over estimated the width of the isotopic distributions while the abrasion-ablation calculation[42] was in reasonable agreement with the data. Therefore, it is interesting to see if the disagreement between the two models increases as the mass number of the fragmenting nucleus is increased.

The collision of the RHI projectile with the target nucleus is treated as a two step process in the Monte Carlo cascade calculation, a fast step with cascading collisions of nucleons from one reaction partner inside the nucleus of the other partner, and a slow statistical evaporation step of the primary fragments after the fast cascading nucleons have escaped or have been captured by the primary fragments. The calculation is made using an extension of the intranucleon cascade code [44], VEGAS, for proton induced reactions which has been modified to treat two colliding nuclei.[41] The calculations were performed with step function density distributions for both nuclei and without refraction and reflection at the nuclear boundaries for the cascading particles. Fermi motion was included in the projectile as well as in the target nucleus. An infinite rearrangement time was assumed for the time necessary for the nucleus to respond to the removal of nucleons from the Fermi sea by the fast cascade. Meson production and cascades were included via the ISOBAR model.[45] The impact parameter for each collision was selected at random, and the final production cross sections were integrated over impact parameter.

The primary fragments from the fast cascade are subsequently individually deexcited using a version of the Dostrovsky, Fraenkel and

Friedlander statistical model Monte Carlo calculations.[46,41] The excitation energy of each fragment was obtained from the fast cascade code. The absolute value of mass distribution of the final products, i.e. after statistical evaporation, from the reaction of 8 GeV ^{20}Ne with ^{181}Ta is shown in Fig. 8 by the histograms. For clarity the calculated values of the mass yield have been averaged into 5 amu wide bins. The uncertainties shown reflect the uncertainties in the statistics of the calculations and not the uncertainties in the averages.

For comparison with the calculations the measured mass yield results for this system are shown by the dotted curve in Fig. 8. This curve was drawn smoothly through the data points of Fig. 6 by eye. Several features of the comparison with the cascade calculation are worth noting: (a) the absolute normalization of the cross section for the production of heavy products is approximately correct, but is $\sim$25% too large on the average. (b) The general shape of the residue distribution is also approximately correct in the region above mass number 100. However, below mass number 100 the data and the calculation diverge. The cascade-evaporation calculation first predicts more cross section than is observed (nearly a factor of 2 at A $\sim$95) and then drops off to zero cross section before A $\sim$50.

In the abrasion-ablation view of the collision of the RHI with a target nucleus[16-18] the two nuclei are taken to be hard spheres which move on straight line trajectories. Those nucleons that lie in the region of overlap of the two nuclei are sheared off in the abrasion (or fast) stage of the collision. The spectator fragments of the target (and projectile) which consist of the nucleons that

were outside the region of overlap are then assigned an excitation energy that is proportional to their excess surface area. The neutron to proton ratio of the removed nucleons is taken to be equal to that of the target (or projectile) and the variance in the ratio is calculated from the zero point quantum vibrations of the giant dipole resonance (GDR).[18] The oscillator spring constant for this vibration was taken from the liquid droplet model of the GDR.[47] This calculation can be viewed as a leading term approximation to the correlated model of Bondorf et al.[19] in which higher order vibrations are included. The primary products are then allowed to deexcite through a statistical evaporation chain with neutron, proton and alpha emission, and fission competition.[18]

The results of these calculations are shown in Fig. 8 by the solid line. We have arbitrarily cut off the calculations at A $\sim$110 because products with lower mass numbers arise from collisions in which the hard sphere nucleus of the projectile sweeps a cylindrical hole through the target nucleus (removing some 40 nucleons and leaves a "donut-shaped" nucleus with some $\sim$250 MeV of excitation energy due to its increased surface area). It is doubtful whether such nuclei are created and should be considered, rather, as a region outside the limitations of the original model.[16] As with the cascade calculation the absolute magnitude of the mass yield cross section is overestimated by the abrasion-ablation calculation. However, the cross section is over estimated by a factor of $\sim$2 in the latter case, a much larger discrepancy than that for the former calculation. The general shape

of the distribution of high mass (i.e. peripheral collision) products is reproduced.

From the comparisons shown in Fig. 8 one can see that both models can predict the general shape of the mass yield curve for high mass products but miss the absolute cross section. Neither calculation can reproduce the mass yields observed for low mass products. That is, neither calculation produces the low mass products observed in the experiment. This discrepancy was hinted at in the study of Porile et al.[43] with a Ag target nucleus but is dramatized in the results with Ta target.

A more stringent test of the two reaction models can be made by comparison of the predicted isotopic production cross sections, $d^2\sigma/dZdA$, with the experimental data. A significant difference between the two calculations that is visible in the isotopic cross sections is the amount of correlation of the neutrons and protons that are removed in the fast stage of the reaction. The cascade calculation has no correlations at all as the neutron or proton nature of the cascading nucleons is selected at random in proportion to their number in the nucleus. On the other hand, the nucleons removed in the abrasion-ablation calculations are highly correlated.[42,18] The difference between the final products of the two calculations have been shown to be small for low mass nuclei[37] but should be large in high mass nuclei. Figure 9 shows the calculated final isotropic production cross sections for lutetium and hafnium products from the reaction of 8 GeV ^{20}Ne with ^{181}Ta. The irregularities in the curves show the effects of the variation of excitation energy and irregularities in

the mass surface on the statistical deexcitation process. The difference in the widths of the two distributions is dramatic, especially for these peripheral collision products. This difference stems from both initial the removal of nucleons in an uncorrelated fashion and the delivery to the target nucleus of large amounts of excitation energy with little removed mass by the cascade calculation. Comparison with the experimental data (cf. either Fig. 5 or Fig. 10) shows that the cascade calculation grossly over estimates the widths of the experimental isotopic distributions. This must be due, in part, to a lack of correlations in the nucleus. In fact, neither calculation is able to reproduce the measured isotopic distributions although the abrasion-ablation calculation does describe modestly well the width of the distribution. In Fig. 10A we present the comparison of the abrasion-ablation calculation to the measured isotopic distributions for the $\Delta Z = 1$ and 2 products from the $^{20}Ne + {}^{181}Ta$ system. One sees that the calculations fail to reproduce both the absolute value and the centroid of the distributions. The difference in the absolute normalization was seen before in the comparisons to the mass yield calculations. The difference between the centroids of the calculated and measured distributions may be easily understood.

The excitation energies of the primary fragments produced in the abrasion-ablation model are merely those due to the increased surface area of the fragments. This excitation clearly should be viewed as a lower limit to the true excitation of such fragments. Two very likely sources of excitation of the spectator fragments are any frictional forces acting during the abrasion process and scattering

of the participant nucleons into the spectator pieces.[17] To explore the magnitude of these excitation energies we have increased the values of the primary fragment excitation energies until the centroids of the calculations match those of the measured products. The results of this process are shown in Fig. 10A by the solid squares. The primary fragments were raised to a uniform excitation energy of ∿75 MeV. Extension of these comparisons to products with lower masses was not made because of a lack of data for these products.

In Fig. 10B we show the results of a similar analysis of the near target residues from the reaction of ^{20}Ne and ^{197}Au. The features observed with the products from the ^{181}Ta target are analogously obtained with the slightly larger target nucleus. In order to match the centroids of the iridium and platinum distributions, the excitation energies of the primary fragments had to be raised to ∿60 MeV. The difference between this value and the value of ∿75 MeV for the products from ^{181}Ta may not be significant as it depends on the details of the deexcitation calculation. Thus, we have shown that the near target residues from the reaction of ^{20}Ne with ^{181}Ta and ^{197}Au are not accurately described by the Monte Carlo cascade calculation or by the abrasion-ablation calculation. However, the abrasion-ablation calculation can be brought into closer agreement if the excitation energies of the primary fragment are raised to ∿60 to ∿75 MeV.

IV. CONCLUSIONS

This study of the reaction of 8.0 GeV ^{20}Ne with ^{181}Ta and ^{197}Au has shown that several features of the reaction processes occurring in RHI collisions may be best explored with high mass targets. Our results show that the total energy of the projectile is a better parameter for describing the mass yield curve than the projectile velocity for high mass targets. This is a confirmation of the results of Cumming et al. obtained with low mass targets.[5,10] This can be viewed as the onset of limiting fragmentation in these reactions, or perhaps more enlightening, as evidence for the dominating effect of the statistical deexcitation process on the mass yield curve. This domination can remove large differences in the distributions of highly excited primary fragments of the initial encounter.[37] Comparison of the mass yield curve to two reaction models, a Monte Carlo intranuclear cascade-model[41] and an abrasion-ablation model[42], shows that neither model predicts the existance of low mass products; although, both generate approximately the correct shape for high mass product distribution. These differences are much more pronounced than those seen in the fragmentation of lighter nuclei.[37,43] Integration of the mass yields for nuclei with A >40 shows that ∿75 percent of the hard sphere reaction cross section[39,26] (∿80 percent of the soft sphere model[40]) is accounted for in such products. This indicates that collisions in which the central density of the projectile lies inside the hard sphere radius of the target contribute to these products. Therefore, more-central collisions give rise to heavy residues in these collisions than with lighter nuclei. Finally, neither reaction model calculation

was able to reproduce the near-target isotopic production cross sections for either target. In the case of the cascade calculation this may be due to the lack of correlations of the nucleons in the nuclear ground state. The abrasion-ablation calculation fails to reproduce the absolute values of the cross sections as well as the centroids of the isotopic distributions. The former problem may be an indication of the breakdown of the assumption of straight line trajectories in the model, while the latter deficiency has been shown to be due to an underestimation of the excitation energies of the primary fragments.

ACKNOWLEDGEMENTS

We would like to acknowledge the efforts of Dr. R. J. Otto in the development of the mass yield analysis code and helpful discussions during the course of this work. We would also like to acknowledge the staff of the BEVALAC where the irradiations were performed, especially W. Everette and F. Lothrop.

This work was supported by the U. S. Department of Energy, Nuclear Physics Division, under contract No. W-7405-ENG-48.

REFERENCES

* Work supported by the Nuclear Physics Division of the U.S. Department of Energy.

** Permanent address, Department of Chemistry, Oregon State University, Corvallis, Oregon 97331.

*** Permanent address, Laboratoire Rene Bernas, BP1, 91406 Orsay, France.

1. H. A. Grunder, W. D. Hartsough and E. J. Lofgren, Science 174, 1128 (1971).

2. R. Stock and A. M. Poskanzer, Nucl. Part. Phys. 7, 47 (1977).

3. D. E. Greiner, P. J. Lindstrom, H. H. Heckman, Bruce Corfa, and F. S. Bieser, Phys. Rev. Lett. 35, 152 (1975).

4. J. Gosset, H. H. Gutbrod, W. G. Meyer, A. M. Poskanzer, A. Sandoval, R. Stock and G. D. Westfall, Phys. Rev. C16, 629 (1977).

5. J. B. Cumming, R. W. Stoenner and P. E. Haustein, Phys. Rev. C14, 1554 (1976).

6. C. R. Rudy and N. T. Porile, Phys. Lett. 59B, 240 (1975), and N. T. Porile, G. D. Cole and C. R. Rudy, Phys. Rev. C, submitted for publication, 1979.

7. W. Loveland, R. J. Otto, D. J. Morrissey and G. T. Seaborg, Phys. Lett. 69B, 284 (1977).

8. W. Loveland, R. J. Otto, D. J. Morrissey and G. T. Seaborg, Phys. Rev. Lett. 39, 320 (1977).

9. N. K. Glendenning and Y. Karant, Phys. Rev. Lett. 40, 375 (1978).

10. J. B. Cumming, P. E. Haustein, T. J. Ruth and G. J. Virtes, Phys. Rev. C17, 1632 (1978).

11. J. B. Cumming, P. E. Haustein, and R. W. Stoenner, Phys. Rev. C10, 739 (1974).

12. W. D. Myers, Nucl. Phys. A296, 177 (1978).

13. J. Gosset, J. I. Kapusta and G. D. Westfall, Phys. Rev. C18, 844 (1978).

14. W. E. Nervik and G. T. Seaborg, Phys. Rev. 97, 1092 (1955).

15. J. R. Grover, Phys. Rev. 126, 1540 (1957).

16. J. D. Bowman, W. J. Swiatecki and C. F. Tsang, Lawrence Berkeley Laboratory Report No. LBL-2908, 1973, unpublished; J. Hufner, K. Schafer and B. Schurman, Phys. Rev. C12, 1888 (1975).

17. J. O. Rasmussen, R. Donagelo and L. F. Oliveira, Proc. IPRC Symp. on Macroscopic Features of Heavy Ion Collisions and Pre-equilibrium Processes, Hakone, 1977 (unpublished); L. F. Oliveira, R. Donangelo, and J. O. Rasmussen, Phys. Rev. C19, 826 (1979).

18. D. J. Morrissey, W. R. Marsh, R. J. Otto, W. Loveland and G. T. Seaborg, Phys. Rev. C18, 1267 (1978).

19. J. P. Bondorf, G. Fai and O. B. Nielsen, Phys. Rev. Lett. 41, 391 (1978); Nucl. Phys. A312, 149 (1978).

20. D. J. Morrissey, W. Loveland and G. T. Seaborg, Z. Phys. A289, 123 (1978).

21. C. J. Orth, H. A. O'Brien Jr., M. E. Schillaci, B. J. Dropesky, J. E. Cline, E. B. Nieschmidt, and R. L. Brodzinski, J. Inorg. Nucl. Chem 38, 13 (1976).

22. J. B. Cumming, Ann. Rev. Nucl. Sci. 13, 261 (1963).

23. W. L. Everette, private communication.

24. L. C. Northcliffe and R. F. Schilling, Nucl. Data Tables 7, 233 (1970).

25. L. C. Northcliffe, Ann. Rev. Nucl. Sci. 13, 67 (1963).

26. H. H. Heckman, D. E. Greiner, P. J. Lindstrom and H. Shwe, Phys. Rev. C17, 1735 (1978).

27. D. J. Morrissey, D. Lee, R. J. Otto and G. T. Seaborg, Nucl. Inst. Meth., 158, 499 (1978).

28. J. T. Routti and S. G. Prussin, Nucl. Inst. Meth. 72, 125 (1969).

29. See, for example, P. R. Bevington, Data Reduction and Error Analysis for the Physical Sciences (McGraw-Hill, New York, 1969), p. 200.

30. G. Rudstam, Z. Naturforsch. 21a, 1027 (1966).

31. P. E. Haustein and T. J. Ruth, Phys. Rev. C18, 2241 (1978).

32. S. B. Kaufman, M. W. Weisfield, E. P. Steinberg, B. D. Wilkins and D. Henderson, Phys. Rev. C14, 1121, (1976).

33. J. Hudis, T. Kirsten, R. W. Stoenner, and O. A. Schaeffer, Phys. Rev. C1, 2019 (1970).

34. See, for example, V. E. Ross and K. Bachmann, J. Inorg. Nucl. Chem. 21, 13 (1974), and references therein.

35. H. Boggild and T. Ferbel, Ann. Rev. Nucl. Sci. 24, 451 (1974).

36. See, for example, H. H. Heckman, H. J. Crawford, D. E. Greiner, P. J. Lindstrom, and L. W. Wilson, Phys. Rev. C17, 1651 (1978); and G. D. Westfall, L. W. Wilson, P. J. Lindstrom, H. J. Crawford, D. E. Greiner and H. H. Heckman, Phys. Rev. C19, 1309 (1979); and references therein.

37. D. J. Morrissey, L. F. Oliveira, J. O. Rasmussen, G. T. Seaborg, Y. Yariv and Z. Fraenkel, Lawrence Berkeley Laboratory Report No. LBL-8964, 1979, submitted for publication.

38. H. Feshbach and K. Huang, Phys. Lett. 47B, 300 (1973).

39. H. L. Bradt and B. Peters, Phys. Rev. 77, 54 (1950).

40. P. J. Karol, Phys. Rev. C11, 1203 (1975).

41. Y. Yariv and Z. Fraenkel, to be published.

42. The specific form of the abrasion-ablation model used in the comparison was that of reference 18.

43. N. T. Porile, G. D. Cole and C. R. Rudy, Phys. Rev. C, submitted for publication, 1979.

44. K. Chen, Z. Fraenkel, G. Friedlander, J. R. Grover, J. M. Miller, and Y. Shimamoto, Phys. Rev. 166, 949 (1968).

45. G. D. Harp, K. Chen, G. Friedlander, Z. Fraenkel, and J. M. Miller, Phys. Rev. C8, 851 (1973).

46. I. Dostrovsky, Z. Fraenkel and G. Friedlander, Phys. Rev. 116, 683 (1959).

47. W. D. Myers, W. J. Swiatecki, T. Kodama, L. J. El-Jaick, and E. R. Hilf, Phys. Rev. C15, 2032 (1977).

FIGURE CAPTIONS

Fig. 1. Large differences in the product mass yield ($d\sigma/dA$) obtained as a function of incident proton energy are shown by the work of Nervik and Seaborg[14] (340 MeV) and Grover[15] (5.7 GeV).

Fig. 2. A schematic diagram of the target arrangement used in the bombardment with ^{20}Ne projectiles at the BEVALAC is shown.

Fig. 3. The ratio of the production cross sections measured with the thick ^{197}Au target to those measured with the thin ^{197}Au are plotted versus the radionuclides' mass number. The solid line at R = 1 represents the value of this ratio that would be expected if there was no contribution from secondary particle induced reactions. The dashed curve is discussed in the text.

Fig. 4. A comparison of the charge dispersion curve for the low mass products, $30 \leqslant A \leqslant 50$, observed in this work (solid curve) with the charge dispersion curve previously measured for products in the same mass range produced in the reaction of 80 BeV ^{40}Ar, 3.9 GeV ^{14}N, 3.9 GeV ^{1}H and 1.57 GeVπ^- - with copper[10,11,31] (dotted curve). The latter curve has been arbitrarily normalized to convert the reported values of fractional chain yields into isotopic production cross sections, $d^2\sigma/dZdA$.

Fig. 5. The charge dispersion curves obtained in this work are shown as a function of mass region of the products. The parameters that describe the center and width of the individual curves are given in Table IV.

Fig. 6. The target residue mass distribution, $d\sigma/dA$, obtained for the reaction of relativistic projectiles with a ^{181}Ta target is shown.

Fig. 7. Similar to Fig. 6, the mass distribution obtained for the 8 GeV $^{20}Ne^{+}$ ^{197}Au target is plotted. For comparision, the data of Kaufman et al.[32] for 11.5 GeV protons (solid squares) plus ^{197}Au and the data of Hudis et al.[33] for 29 GeV protons plus ^{197}Au (solid triangles) are also shown.

Fig. 8. A comparison of the mass yield curve measured in this work (dotted) with the predictions of the Monte Carlo cascade model[41] (histogram) and with the predictions of the abrasion-ablation model[42] (solid curve).

Fig. 9. Calculated final product isotopic distributions are shown for the reaction of ^{20}Ne + ^{181}Ta to produce lutetium and hafnium isotopes. The solid line is from the abrasion-ablation model[42] and the histograms from the cascade model.[41]

Fig. 10. The isotopic production cross sections from the abrasion-ablation model (triangles) are compared to the measured data (solid points) for the reaction of ^{20}Ne with ^{181}Ta, (A), and ^{197}Au, (B). The results for the deexcitation of more highly excited primary products as discussed in the text are shown for both target nuclei (solid squares).

Table I. Irradiation conditions, target thickness and approximate values of the beam degradation by the target foils.

Target	Foil Thickness (mg/cm^2)	Average Flux (particles/min)	Length of Bombardment (minutes)	Energy Loss in Target MeV (percent)	Nuclear Reaction Attenuation ϕ'/ϕ
Au-I	49.3	7.19×10^9	612	<15 (<0.2)	∿.9994
Au-II	242.0			<60 (<0.7)	∿.997
Ta	154.1	1.64×10^{10}	247	<40 (<0.5)	∿.998

Table II. Cross Sections (in millibarns) observed in this work.

Nuclide	Type[a]	Target		
		49.3 mg/cm^2 Au	242 mg/cm^2 Au	154 mg/cm^2 Ta
^{7}Be	C	---	---	37.6 ± 2.5
^{24}Na	C	---	33.4 ± 3.3	28.9 ± 2.9
^{28}Mg	C	7.5 ± 2.0	---	5.7 ± 0.75
^{41}Ar	C	18.3 ± 1.8	17.8 ± 1.8	---
^{42}K	I	---	9.04 ± 0.9	7.4 ± 0.7
^{43}K	C	---	---	54.5 ± 14.4
^{44}Sc	I	---	1.9 ± 1.5	---
^{44m}Sc	I	---	---	3.2 ± 0.3
^{46}Sc	I	---	9.3 ± 0.9	14.8 ± 3.2
^{48}Sc	I	2.8 ± 0.4	2.8 ± 0.1	2.4 ± 0.4
^{48}V	C	---	3.1 ± 0.3	3.1 ± 0.3
^{51}Cr	C	---	---	6.9 ± 2.8
^{52}Mn	C	---	---	1.66 ± 0.11
^{54}Mn	I	---	9.0 ± 1.3	10.6 ± 1.4
^{58}Co	I	---	5.7 ± 1.4	8.7 ± 0.9
^{59}Fe	C	---	2.8 ± 0.2	2.3 ± 0.2
^{65}Zn	C	---	7.0 ± 1.4	---
^{72}Ga	C	---	---	3.1 ± 1.8
^{72}As	C	6.7 ± 0.6	7.6 ± 1.2	---
^{73}Se	C	3.6 ± 2.0	---	1.8 ± 0.1
^{74}As	I	5.2 ± 0.9	---	4.8 ± 0.6
^{75}Se	C	---	6.4 ± 0.4	7.7 ± 6.1
^{76}As	I	---	---	9.0 ± 0.9
^{77}Br	C	---	4.3 ± 0.8	3.5 ± 0.3
^{82m}Rb	I	---	6.4 ± 0.8	---
^{83}Rb	C	---	8.5 ± 1.2	8.7 ± 0.9
^{84}Rb	I	3.8 ± 1.4	4.1 ± 0.3	2.2 ± 0.3

Table II. (continued)

Nuclide	Type[a]	Target		
		49.3 mg/cm^2 Au	242 mg/cm^2 Au	154 mg/cm^2 Ta
^{86}Zr	C	---	---	4.8 ± 1.1
^{87}Y	C	---	8.1 ± 0.8	---
^{87m}Y	C	---	---	9.8 ± 0.9
^{88}Y	C	---	5.4 ± 0.5	---
^{88}Zr	C	---	7.7 ± 0.7	8.7 ± 0.5
^{89}Zr	C	8.3 ± 0.8	9.2 ± 0.9	8.4 ± 0.8
^{90}Nb	C	7.2 ± 0.7	6.7 ± 0.7	---
^{92m}Nb	I	---	1.6 ± 0.1	---
^{93m}Mo	I	4.1 ± 0.4	---	2.9 ± 0.2
^{95}Tc	C	---	9.0 ± 1.2	10.4 ± 1.3
^{96}Tc	I	---	3.6 ± 1.3	2.8 ± 0.3
^{97}Ru	C	4.0 ± 0.3	4.4 ± 0.3	5.8 ± 0.4
^{101m}Rh	C	6.1 ± 0.8	---	---
^{104}Ag	C	---	5.8 ± 3.0	---
^{106m}Ag	I	---	3.9 ± 1.2	---
^{110m}In	C	---	---	7.4 ± 1.8
^{111}In	C	---	5.3 ± 0.3	6.5 ± 0.4
^{118m}Sb	I	---	8.6 ± 0.8	---
^{119m}Te	C	---	---	2.1 ± 0.4
^{121}Te	C	8.5 ± 0.5	---	12.2 ± 0.7
^{121}I	C	---	10.6 ± 2.3	---
^{122}Xe	C	---	7.2 ± 0.7	10.1 ± 0.7
^{123}I	C	9.1 ± 1.1	8.2 ± 0.7	8.1 ± 0.9
^{125}Xe	C	---	---	8.6 ± 0.8
^{127}Xe	C	---	7.7 ± 0.7	11.5 ± 1.1
^{128}Ba	C	---	---	11.5 ± 2.4
^{129}Cs	C	---	---	16.7 ± 0.9

Table II. (continued)

Nuclide	Type[a]	Target		
		49.3 mg/cm^2 Au	242 mg/cm^2 Au	154 mg/cm^2 Ta
^{131}Ba	C	20.4 ± 1.0	19.5 ± 2.4	21.8 ± 5.1
^{135}Ce	C	---	---	14.7 ± 0.6
^{138m}Pr	I	---	2.5 ± 0.9	---
^{139}Ce	C	---	---	8.4 ± 1.6
^{145}Eu	C	16.1 ± 1.6	---	29.8 ± 3.6
^{146}Eu	C	---	---	21.4 ± 2.1
^{147}Eu	C	---	22.7 ± 3.8	17.0 ± 4.6
^{149}Gd	C	12.1 ± 2.4	---	12.7 ± 8.6
^{150a}Tb	C	---	4.7 ± 0.8	---
^{151}Tb	C	---	10.9 ± 7.3	21.0 ± 16.0
^{152}Tb	C	13.6 ± 6.3	12.0 ± 6.1	36.6 ± 7.5
^{153}Tb	C	---	---	15.9 ± 5.3
^{153}Dy	C	---	---	9.7 ± 2.1
^{155}Tb	C	---	---	6.8 ± 0.6
^{155}Dy	C	13.6 ± 1.4	12.2 ± 1.2	---
^{157}Dy	C	---	---	28.3 ± 1.9
^{160}Er	C	9.0 ± 3.8	12.3 ± 2.9	19.4 ± 3.1
^{161}Er	C	36.0 ± 3.6	30.8 ± 1.7	38.0 ± 22.0
^{165}Tm	C	---	---	41.0 ± 16.0
^{166}Yb	C	29.9 ± 4.1	28.6 ± 2.9	63.0 ± 6.2
^{167}Tm	C	17.0 ± 6.7	15.4 ± 4.9	33.0 ± 1.3
^{169}Yb	C	---	7.4 ± 2.2	---
^{169}Lu	C	---	29.1 ± 2.1	36.0 ± 11.0
^{170}Lu	C	---	27.9 ± 2.1	57.3 ± 1.1
^{170}Hf	C	16.5 ± 8.1	---	36.4 ± 7.2
^{171}Lu	C	19.0 ± 1.9	26.2 ± 5.0	46.7 ± 2.1
^{171}Hf	C	---	---	41.4 ± 3.0

Table II. (continued)

Nuclide	Type[a]	Target		
		49.3 mg/cm^2 Au	242 mg/cm^2 Au	154 mg/cm^2 Ta
^{172}Lu	I	---	---	11.1 ± 1.4
^{172}Hf	C	---	24.5 ± 2.7	---
^{173}Hf	C	---	---	32.8 ± 8.6
^{173}Ta	C	12.0 ± 7.0	9.0 ± 2.8	---
^{174}Ta	C	---	21.1 ± 6.4	---
^{175}Hf	C	---	---	59.5 ± 5.7
^{176}Ta	C	52.0 ± 25.0	53.0 ± 20.0	55.4 ± 2.2
^{177}Ta	C	---	---	16.8 ± 1.7
^{181}Re	C	42.4 ± 8.0	39.1 ± 3.8	---
^{183}Re	C	---	53.0 ± 18.0	---
^{184}Ir	C	18.9 ± 7.0	13.0 ± 4.5	---
^{185}Ir	C	29.2 ± 3.0	---	---
^{187}Ir	C	---	58.0 ± 17.0	---
^{189}Ir	C	42.6 ± 4.1	41.3 ± 3.6	---
^{190}Ir	I	5.5 ± 0.9	5.0 ± 0.46	---
^{192}Ir	I	---	2.8 ± 0.2	---
^{188}Pt	C	32.4 ± 3.0	29.8 ± 2.8	---
^{191}Pt	C	---	60.6 ± 9.2	---
^{191}Au	C	31.7 ± 2.8	---	---
^{194}Au	I	---	56.0 ± 3.8	---
^{196}Au	I	174.0 ± 25.0	181.9 ± 14.4	---
^{198}Au	I	43.1 ± 3.8	16.6 ± 0.8	---

a) Nuclides are typed I or C to indicate either independent yield or partial cumulative yield, respectively. This distinction is discussed in the text.

Table III. Thick to thin target cross section ratio from the ^{197}Au targets.

Nuclide	Ratio $\frac{\sigma\ (242.0\ mg/cm^2\ ^{197}Au)}{\sigma\ (49.3\ mg/cm^2\ ^{197}Au)}$
^{41}Ar	0.97 ± .14
^{48}Sc	1.00 ± .15
^{72}As	1.13 ± .21
^{84}Rb	1.08 ± .41
^{89}Zr	1.11 ± .15
^{90}Nb	0.93 ± .09
^{97}Ru	1.10 ± .11
^{123}I	0.90 ± .13
^{131}Ba	0.96 ± .13
^{152}Tb	0.88 ± .61
^{155}Dy	0.90 ± .13
^{160}Er	1.37 ± .66
^{161}Er	0.86 ± .10
^{166}Yb	0.96 ± .16
^{167}Tm	0.91 ± .46
^{171}Lu	1.38 ± .30
^{173}Ta	0.75 ± .50
^{176}Ta	1.02 ± .62
^{181}Re	0.92 ± .23
^{184}Ir	0.69 ± .35
^{189}Ir	0.97 ± .13
^{190}Ir	0.91 ± .17
^{188}Pt	0.92 ± .12
^{196}Au	1.05 ± .16

Table IV. Charge dispersion parameters.

Mass Range	Target	s_z	$Z_p(A) = a + bA + cA^2$		
			a	b	c
7 - 48	Ta, Au	0.55	0.1	0.456	0
51 - 76	Ta, Au	0.475	1.0	0.436	0
73 - 77	Ta, Au	0.45	-4.9	0.526	0
82 - 88	Ta, Au	0.45	-0.64	0.454	0
86 - 106	Ta, Au	0.45	5.95	0.391	0
110 - 139	Ta, Au	0.45	4.76	0.400	0
145 - 157	Ta Au	0.45	13.2 13.7	0.337	0
160 - 169	Ta Au	0.45	-6.7 -6.6	0.463	0
169 - 177	Ta Au	0.50 0.45	-0.3 0	0.485	-3.8×10^{-4}
181 - 191	Au	0.50	-0.1	0.485	-3.8×10^{-4}

Table V. Total cross section comparison.

	Experimental Large Fragment Cross Section (barns)	Calculated Cross Section (barns)	
		Hard Sphere	Soft Sphere
$^{20}Ne + {}^{181}Ta$	2.8 ± 0.5	3.64	3.47
$^{20}Ne + {}^{197}Au$	2.8 ± 0.5	3.80	3.59

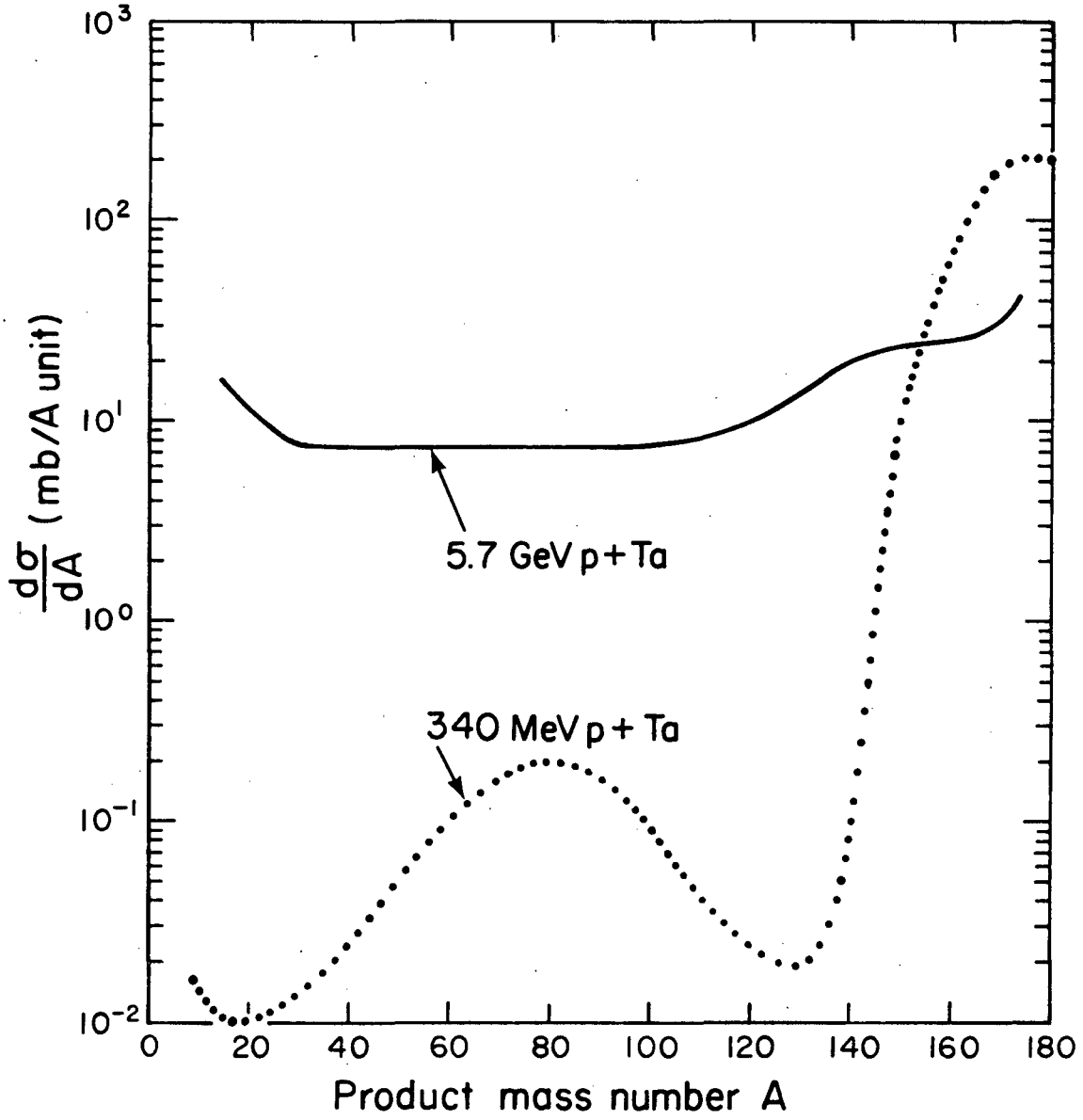
10^3
10^2
10^1
10^0
10^{-1}
10^{-2}
$\frac{d\sigma}{dA}$ (mb/A unit)
5.7 GeV p+Ta
340 MeV p+Ta
0
20
40
60
80
100
120
140
160
180
Product mass number A

XBL 794-1083

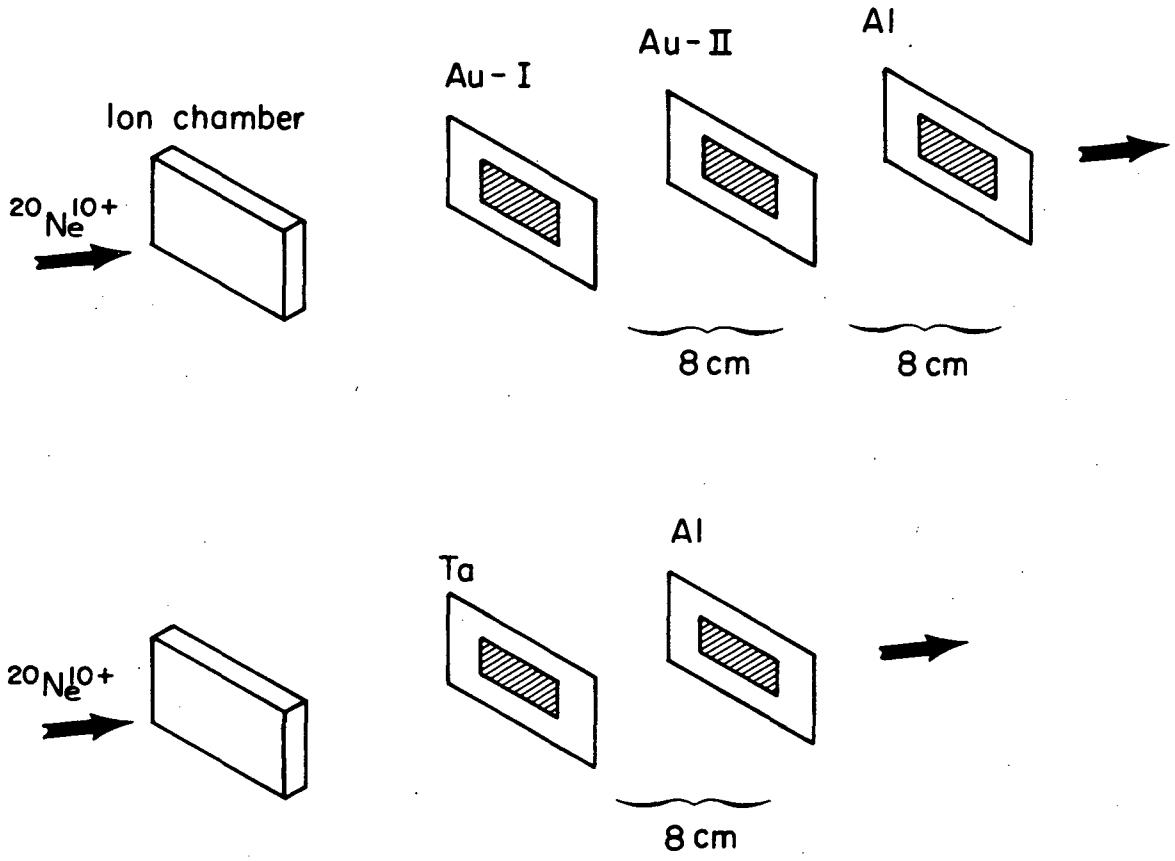

XBL 794-1079

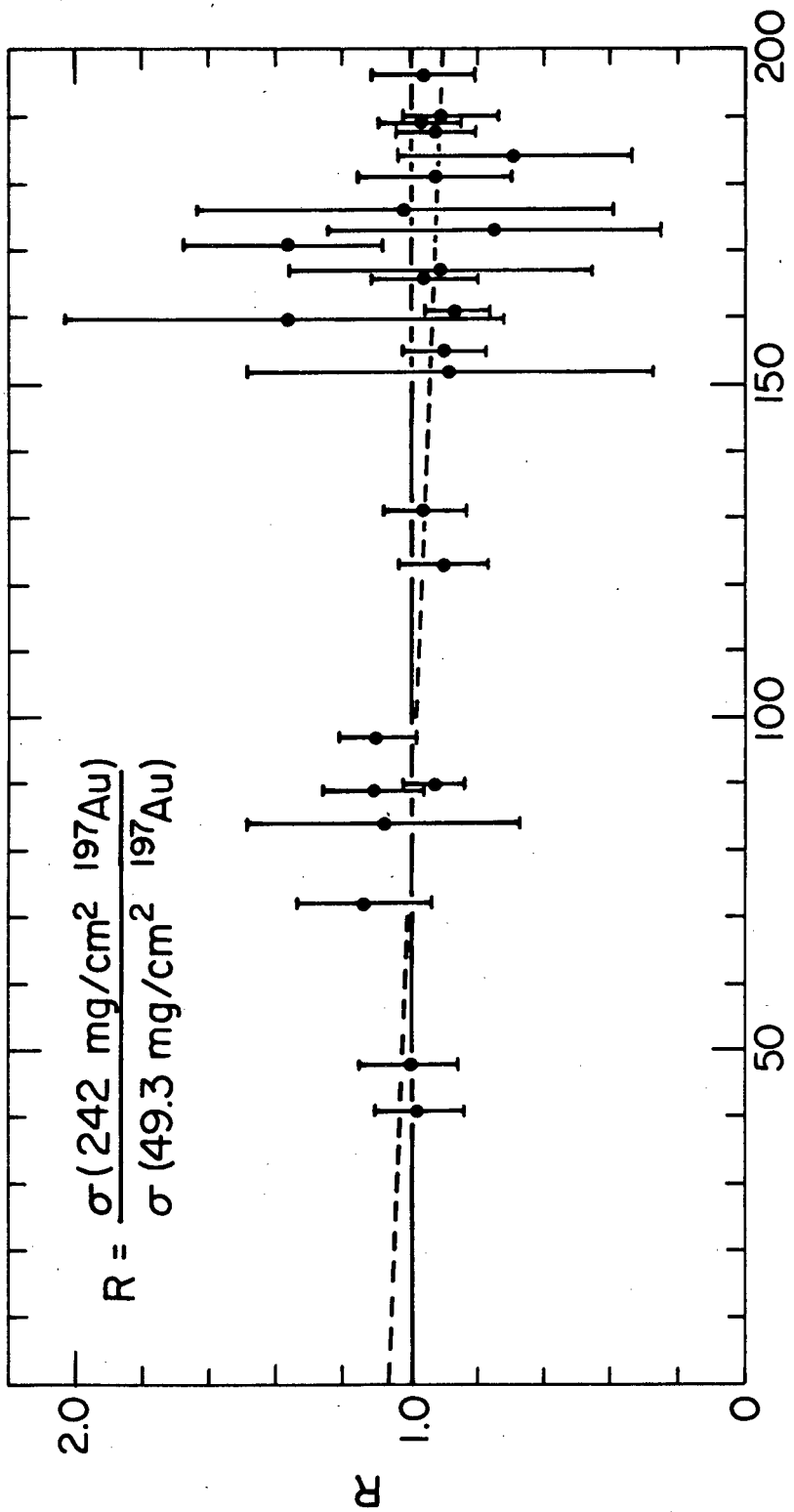
R = σ(242 mg/cm² 197Au) / σ(49.3 mg/cm² 197Au)
R
2.0
1.0
0
50
100
150
200
Mass number, A

XBL 794-1080

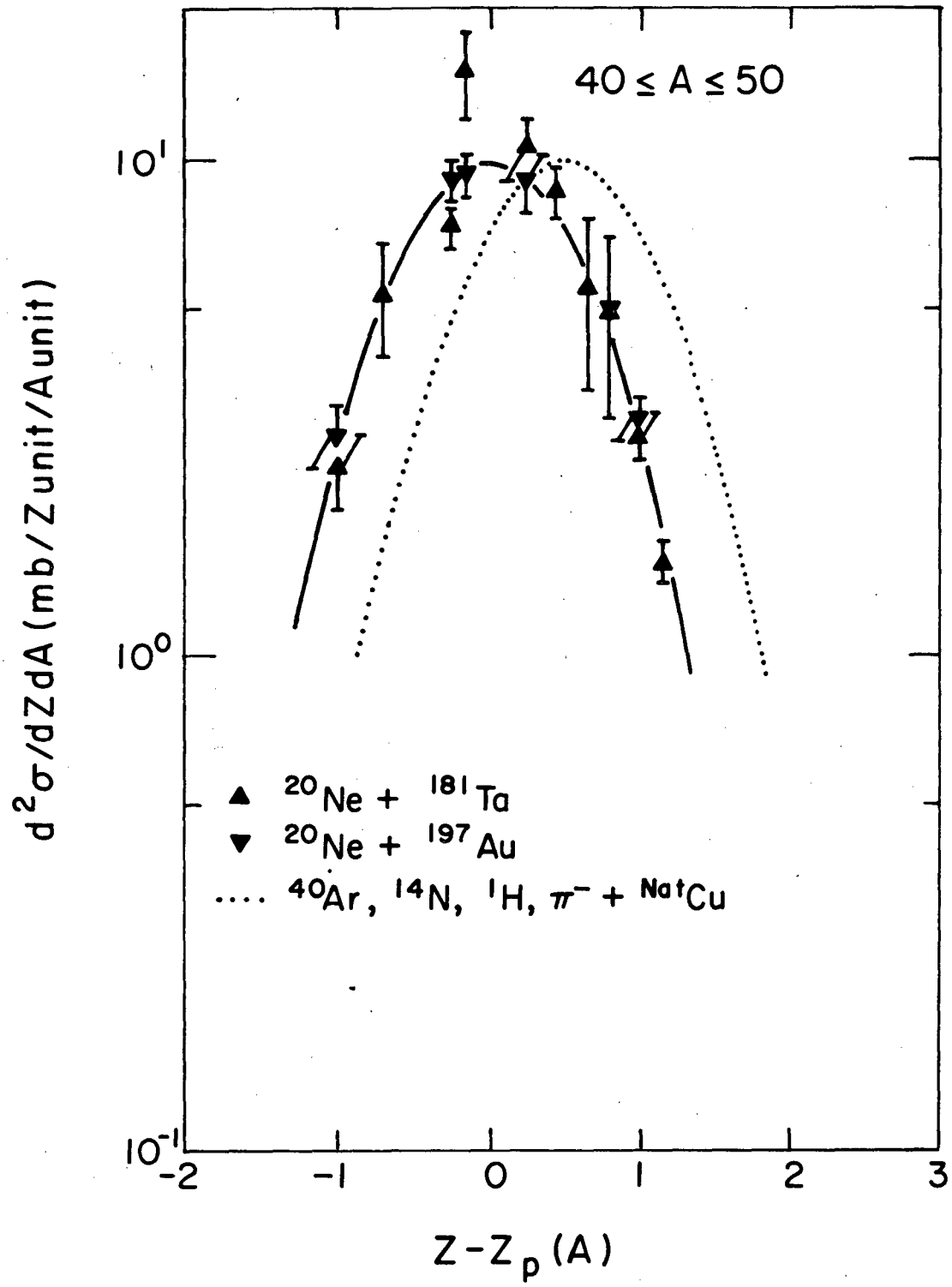
40 ≤ A ≤ 50
10^1
10^0
10^{-1}
$d^2\sigma/dZdA$ (mb/Zunit/Aunit)
▲ $^{20}Ne + {}^{181}Ta$
▼ $^{20}Ne + {}^{197}Au$
···· ^{40}Ar, ^{14}N, ^{1}H, π^- + ^{Nat}Cu
-2
-1
0
1
2
3
$Z - Z_p$ (A)

XBL 794-1082

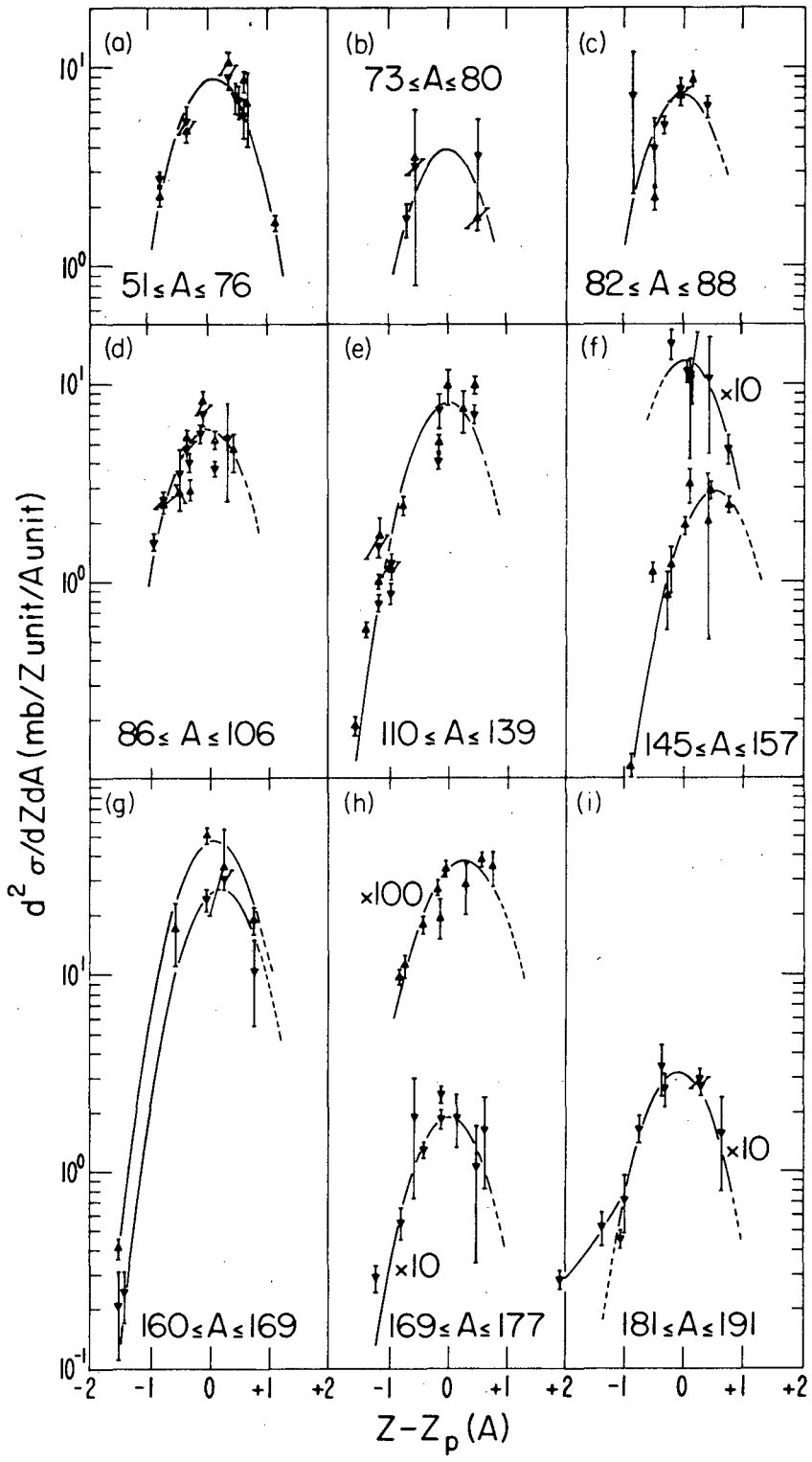
(a)
(b)
73≤A≤80
(c)
51≤A≤76
82≤A≤88
(d)
(e)
(f)
×10
86≤A≤106
110≤A≤139
145≤A≤157
(g)
(h)
(i)
×100
×10
×10
160≤A≤169
169≤A≤177
181≤A≤191
d²σ/dZdA (mb/Z unit/A unit)
Z−Z_p (A)

XBL 794-1078

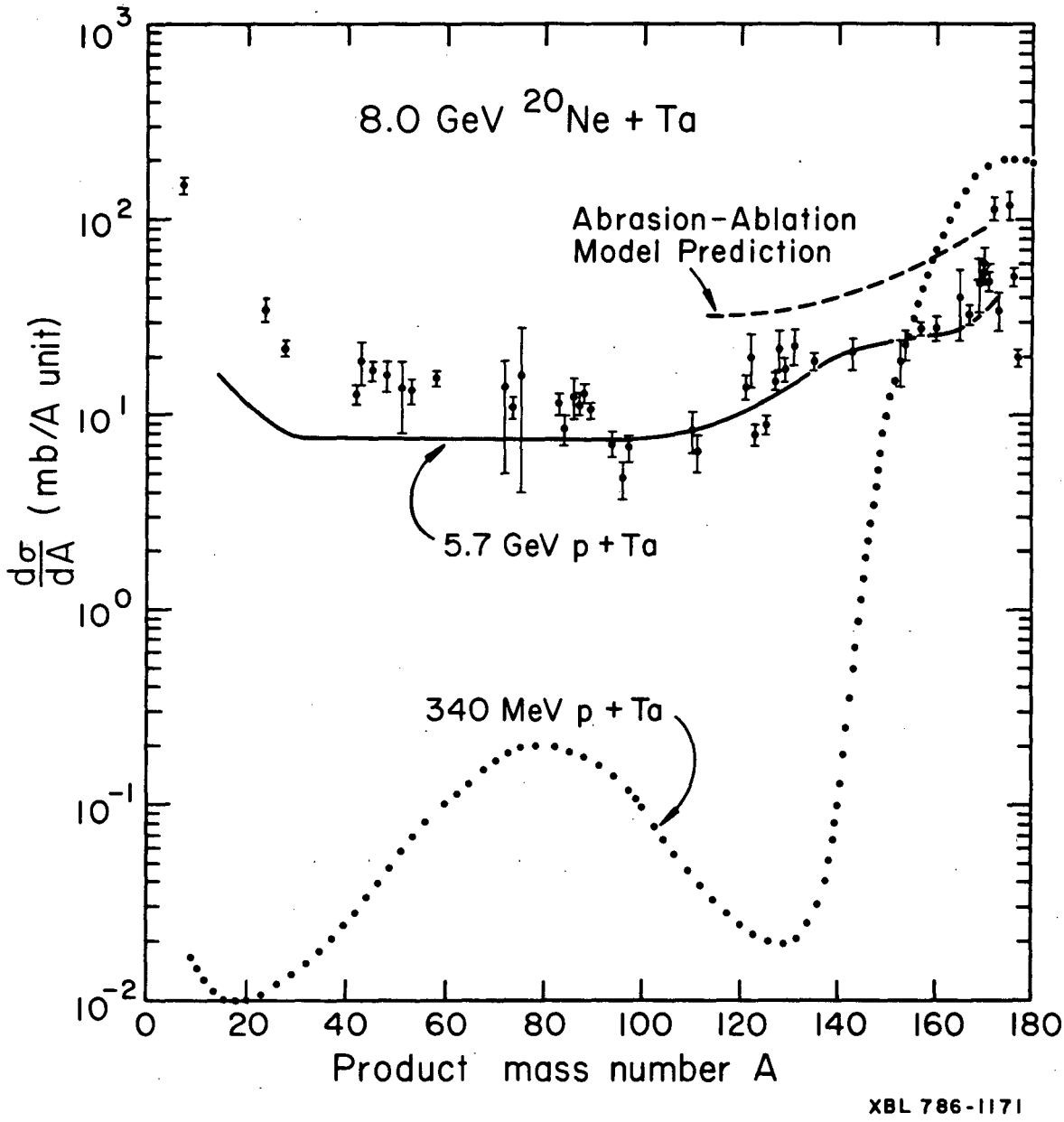
8.0 GeV ^{20}Ne + Ta
Abrasion-Ablation
Model Prediction
5.7 GeV p + Ta
340 MeV p + Ta
$\frac{d\sigma}{dA}$ (mb/A unit)
Product mass number A
XBL 786-1171

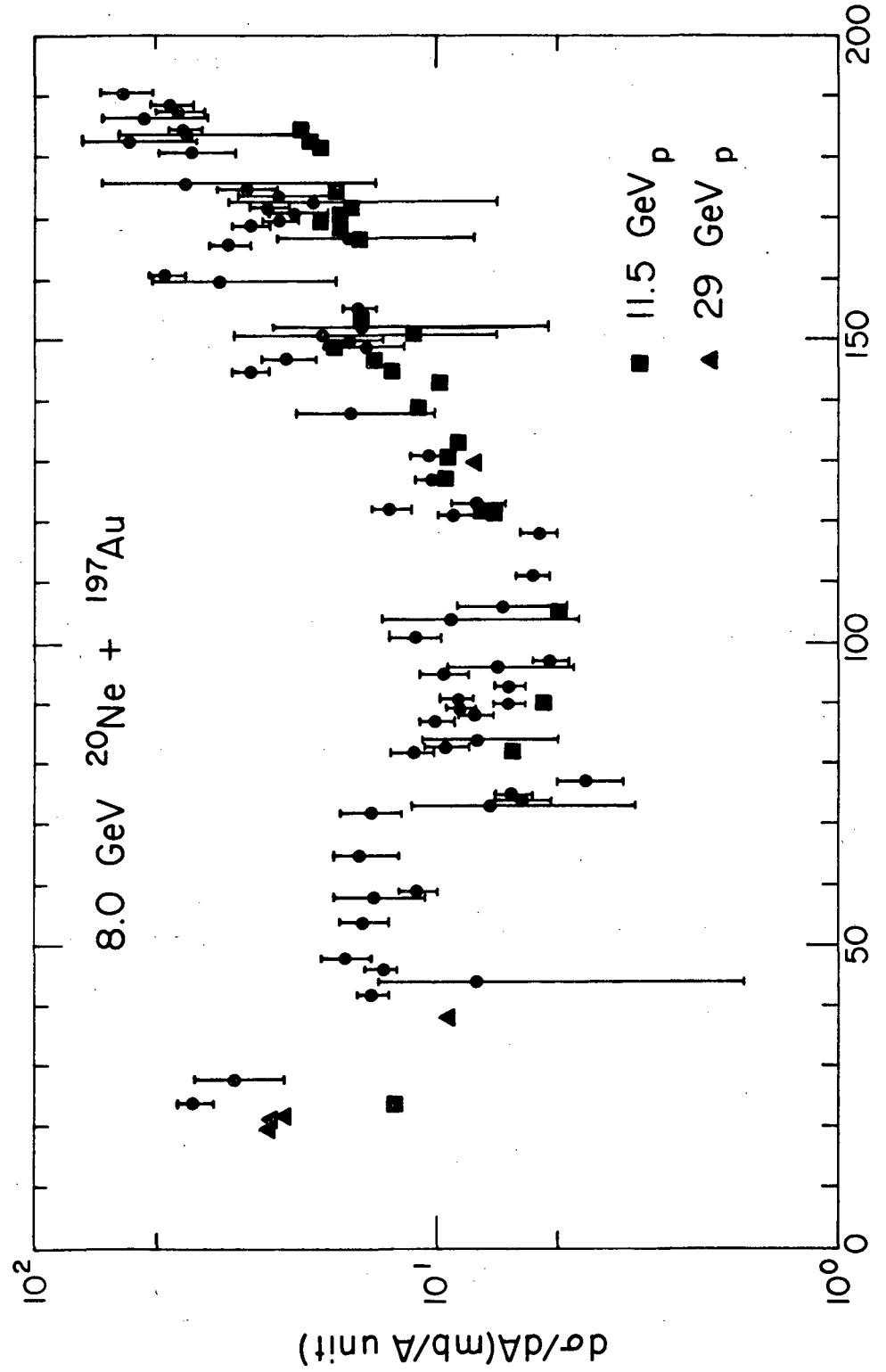
8.0 GeV ^{20}Ne + ^{197}Au
11.5 GeV p
29 GeV p
dσ/dA(mb/A unit)
Product mass number A
10^2
10^1
10^0
0
50
100
150
200

XBL 794-1081

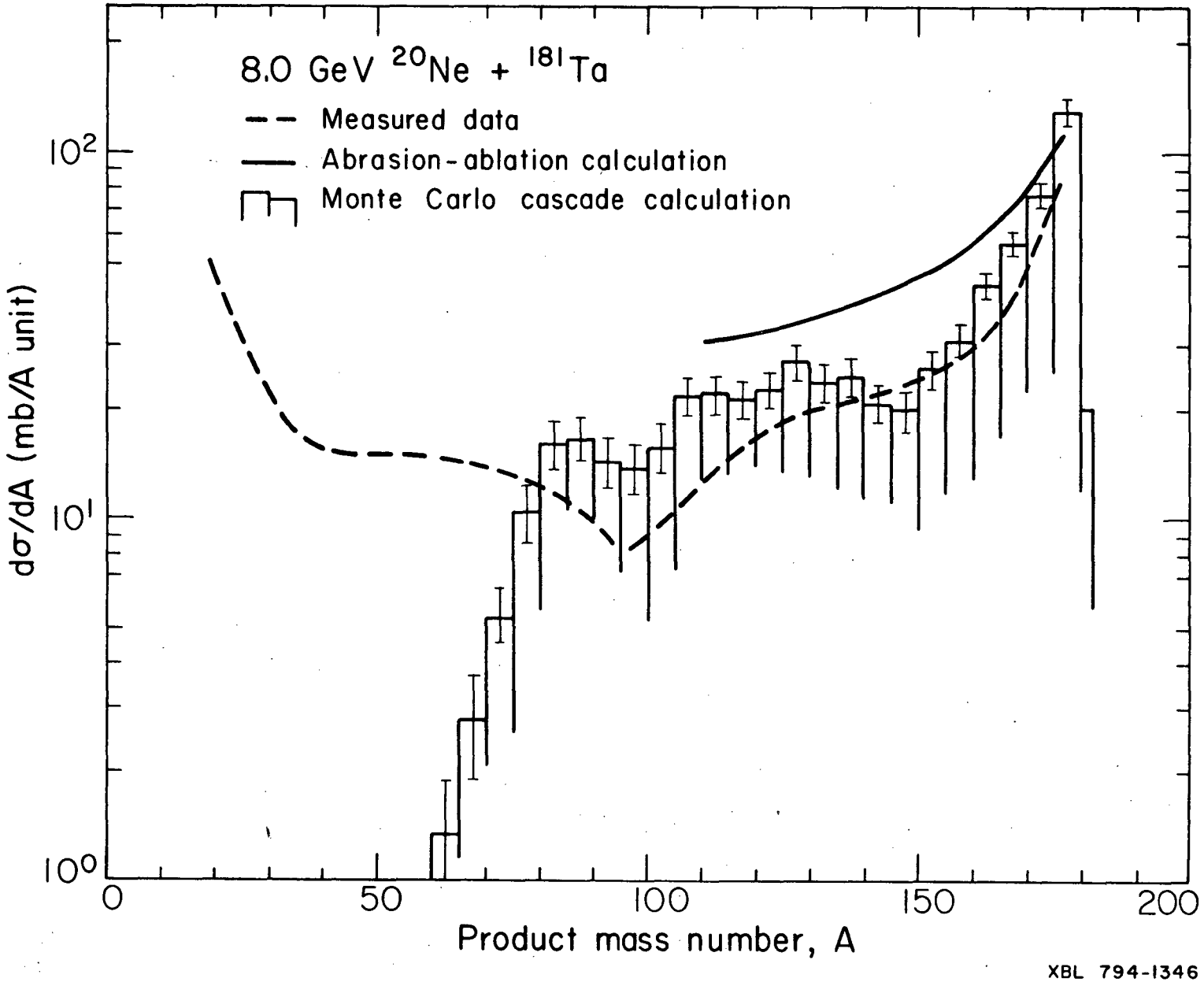
8.0 GeV ^{20}Ne + ^{181}Ta
Measured data
Abrasion-ablation calculation
Monte Carlo cascade calculation
dσ/dA (mb/A unit)
10^2
10^1
10^0
0
50
100
150
200
Product mass number, A
XBL 794-1346

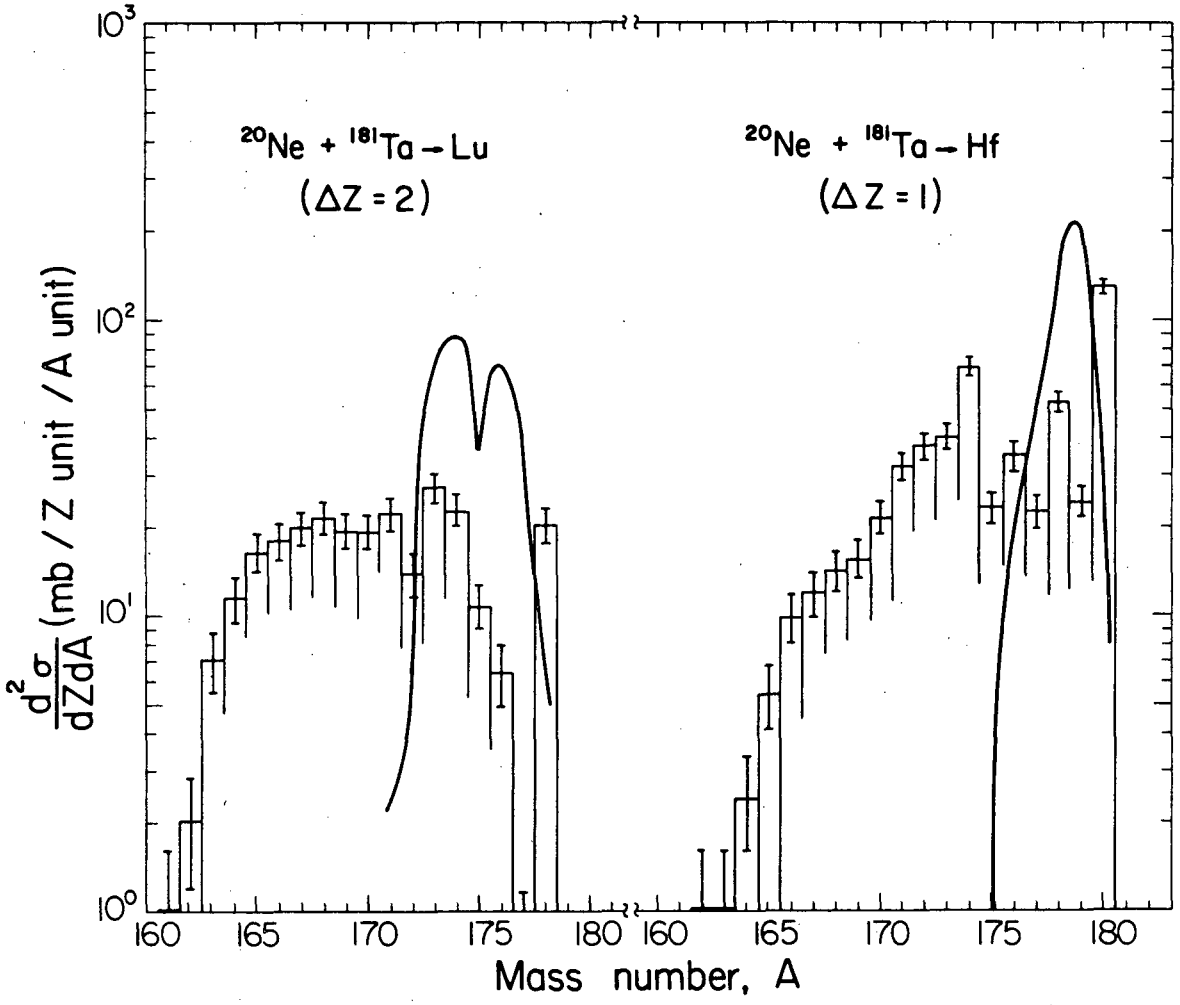
$^{20}Ne + {}^{181}Ta \rightarrow Lu$
$(\Delta Z = 2)$
$^{20}Ne + {}^{181}Ta \rightarrow Hf$
$(\Delta Z = 1)$
$\frac{d^2\sigma}{dZdA}$ (mb / Z unit / A unit)
10^3
10^2
10^1
10^0
160
165
170
175
180
Mass number, A

XBL 793-898

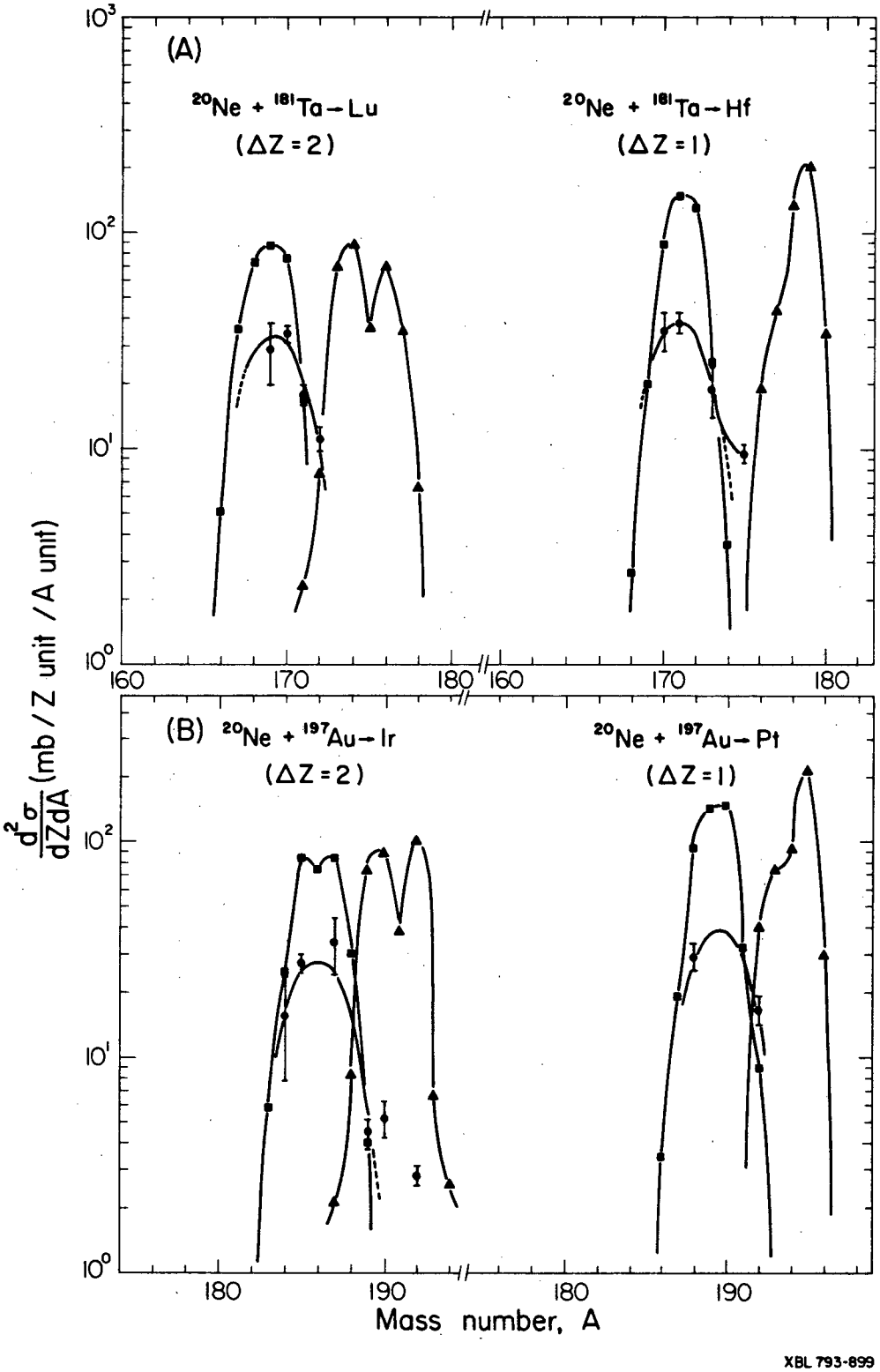
(A)
^{20}Ne + ^{181}Ta → Lu
(ΔZ = 2)
^{20}Ne + ^{181}Ta → Hf
(ΔZ = 1)
(B) ^{20}Ne + ^{197}Au → Ir
(ΔZ = 2)
^{20}Ne + ^{197}Au → Pt
(ΔZ = 1)
$\frac{d^2\sigma}{dZdA}$ (mb / Z unit / A unit)
Mass number, A
XBL 793-899

TECHNICAL INFORMATION DEPARTMENT
LAWRENCE BERKELEY LABORATORY
UNIVERSITY OF CALIFORNIA
BERKELEY, CALIFORNIA 94720